Journal of Applied Fluid Mechanics, Vol. 14, No. 3, pp. 909-920, 2021.
Available online at www.jafmonline.net, ISSN 1735-3572, EISSN 1735-3645.
DOI: 10.47176/jafm.14.03.32062

Improved Simulation of Flows with Free-Surface Waves by Optimizing the Angle Factor in the HRIC Interface-Sharpening Scheme

J. C. Berndt†, R. Perić and M. Abdel-Maksoud

Institute for Fluid Dynamics and Ship Theory, Hamburg University of Technology, Am Schwarzenberg-Campus 4 (C), 21073 Hamburg, Germany

† Corresponding Author Email: j.berndt@tuhh.de

(Received July 30, 2020; accepted November 5, 2020)

ABSTRACT

In finite-volume-based simulations with free-surface waves, it is usually desired to obtain a sharp interface between both fluid phases. A widely used approach for interface-capturing and sharpening is the combination of the volume-of-fluid method with the HRIC scheme. The HRIC scheme contains a user-defined parameter, the angle factor, which influences the magnitude of the interface-sharpening. The present work demonstrates that the optimum value for the angle factor is case dependent: too small values can cause substantial flow disturbances, such as vorticity production within the wave and the occurrence of parasitic wave components, whereas too large values can cause excessive dissipation of wave energy. The optimum value for the angle factor was found to depend on the wave steepness, the aspect ratio of the grid cells, on the cell size and to a lesser degree on the time step size. Results from an extensive parameter study are presented, which can provide guidance for optimizing the angle factor for flow simulations of free-surface wave propagation. Further, two methods are presented which can be used to determine the optimum value of the angle factor. The magnitude of errors that can occur due to improper choices of the angle factor are discussed and recommendations are given to increase the accuracy of flow simulations with free-surface waves.

Keywords: Volume-of-fluid method; Free-surface waves, Interface-capturing; HRIC; Interface-sharpening; Optimizing case-dependent parameters.

NOMENCLATURE

C_R	reflection coefficient	$\boldsymbol{v}$	fluid velocity
C_θ	angle factor	w	velocity component in z-direction
Co	Courant number		
c	wave celerity	α	volume fraction
H	wave height	γ	forcing strength for wave damping
H_0	initial wave height prescribed at the wave inlet	ζ	surface elevation
		Δx	cell size in horizontal direction
$\boldsymbol{n}$	surface normal of the control volume face	Δz	cell size in vertical direction
		θ	interface orientation angle
q	source term	λ	wave length
T	wave period	μ	dynamic viscosity
t	time	ρ	density
u	velocity component in x-direction	$\vec{\omega}$	vorticity
		ω_y	vorticity component around y-axis

1. INTRODUCTION

The simulation of free-surface flows is a challenging topic in computational fluid dynamics and subject to ongoing research. Different approaches describing their flow characteristics can be classified as Lagrangian particle or Eulerian mesh methods. Examples for the recent application of Lagrangian particle methods such as smoothed particle hydrodynamics (SPH) and moving particle simulations (MPS) for free-surface-flow simulations are given by Zheng *et al.* (2020) and Ni *et al.* (2020).

The present work however, focuses on the Eulerian approach given by the finite-volume method (FVM). Finite-volume-based flow solvers using the volume-of-fluid (VOF) method (Hirt and Nichols 1981) are widely used to simulate flows with free-surface waves. The properties of the fluid mixture are determined based on their volume fraction α in the corresponding control volume (CV). The volume fraction α takes a value between 0 and 1, with 0 (or 1) corresponding to a CV filled completely with air (or water). The transport equation for the volume fraction of an incompressible fluid is given by

$$\frac{d}{dt}\int_V \alpha \; dV + \int_S \alpha\,(\boldsymbol{v}-\boldsymbol{v}_g)\cdot\boldsymbol{n}\; dS = \int_V q_\alpha \; dV \qquad (1)$$

with CV volume V, surface S, fluid velocity $\boldsymbol{v}$, grid velocity $\boldsymbol{v}_g$, surface normal $\boldsymbol{n}$ pointing outside the CV and volume fraction sources q_α.

The key difficulty is to maintain a sharp interface between different fluid phases. This problem results from the choice of discretization schemes for the advection term in the conservation equation for the volume fraction α : First-order upwind differences (FUD) are unconditionally stable but they produce artificial numerical diffusion, which can smear the interface. First-order downwind differences (FDD) sharpen the interface but may result in numerical instability and unphysical interface distortions (see Leonard 1991 and Muzaferija and Perić 1998). Higher-order differencing schemes can be reformulated as a combination of FUD and FDD via the Normalized-Variable Diagram (NVD) as was shown by Leonard (1991). Therefore, the problem of maintaining a sharp interface between the fluid phases corresponds to determining the correct blend between FUD and FDD schemes.

A widely used group of approaches for interface-sharpening are the high-resolution schemes based on blending FUD and FDD via the Normalized-Variable Diagram (NVD), such as ULTIMATE (Leonard 1991), SURFER (Lafaurie *et al.* 1994), CICSAM (Ubbink and Issa 1999), HRIC (Muzaferija and Perić 1998) and STACS (Darwish and Moukalled 2006). The approaches differ in their choice of upwind and downwind schemes and their blending criteria. There are several publications that compare the performance of different high-resolution schemes for particular applications (e.g. Darwish and Moukalled 2006 and Wacławczyk and Koronowicz 2008). However, it appears that no single scheme is superior, since different schemes provided the best results for different test cases.

These high-resolution schemes usually include parameters which can be modified to optimize the interface-sharpening for the specific application. A significant drawback is that optimum values are not readily available and therefore have to be determined by extensive trial-and-error testing.

The aim of this paper is to provide guidance for estimating the optimum value for these parameters for the simulation of free-surface waves. For this purpose methods and results are presented for the evaluation of the quality of the interface-sharpening.

The present work focuses on the HRIC scheme in finite-volume-based flow simulations of free-surface waves. The HRIC scheme contains the user-defined parameter C_θ (angle factor) and is described in section 3. Methods for determining optimum values of C_θ are introduced in section 5. Section 6 presents results of an extensive parameter study for flow simulations with regular free-surface wave propagation, based on the setup described in section 4. The influence of the angle factor is analyzed for different cell sizes and cell aspect ratios of the numerical grid near the interface. Section 7 discusses the implications of the results and presents recommendations for engineering practice.

2. GOVERNING EQUATIONS

The two fluid phases are treated with the volume-of-fluid (VOF) method as one incompressible fluid mixture obeying the same set of governing equations for mass and momentum conservation:

$$\int \rho\boldsymbol{v}\cdot\boldsymbol{n}dS = 0 \quad , \qquad (2)$$

$$\frac{\partial t}{\partial}\int_V \rho\, u_i dV + \int_S \rho\, u_i \boldsymbol{v}\cdot\boldsymbol{n}dS = \int_s(\tau_{ij}\boldsymbol{i}_j - p\boldsymbol{i}_j)\cdot dS + \int_V \rho\,\boldsymbol{g}\cdot\boldsymbol{i}_i dV + \int_V \rho\, q_i dV, \qquad (3)$$

with the volume V of the control volume, its surface S, fluid velocity $\boldsymbol{v}$ with cartesian components u_i, surface normal $\boldsymbol{n}$ (pointing outwards of the CV), time t, density ρ, momentum source terms q_i, the components of the viscous stress tensor τ_{ij}, unit vector $\boldsymbol{i}_j$ for the jth direction and gravitational acceleration $\boldsymbol{g}$.

The fluid properties density ρ and viscosity μ of the fluid mixture are determined as the weighted average based on the volume fraction α :

$$\rho = \alpha\rho_{\text{water}} + (1-\alpha)\rho_{\text{air}}, \qquad (4)$$

$$\mu = \alpha\mu_{\text{water}} + (1-\alpha)\mu_{\text{air}}, \qquad (5)$$

in terms of the phase densities $\rho_{\text{water}} = 1000\ \text{kg/m}^3$ and $\rho_{\text{air}} = 1.2\ \text{kg/m}^3$ and the viscosities $\mu_{\text{water}} = 8.9\cdot10^{-4}\ \text{Pa}s$ and $\mu_{\text{air}} = 1.86\cdot10^{-5}\ \text{Pa}s$. The volume fraction is defined as described in section 1.

Wave damping at the outlet boundary is implemented by defining the source terms q_α in Eq. (1) and q_i in Eq. (3) within the forcing zone:

$$q_\alpha = \gamma b(\boldsymbol{x})(\alpha_{\text{ref}} - \alpha), \qquad (6)$$

$$q_i = \gamma b(\boldsymbol{x})(u_{i,\text{ref}} - u_i), \qquad (7)$$

with blending strength γ, blending function $b(\boldsymbol{x})$ and the volume fraction α_{ref} and velocity components $u_{i,\text{ref}}$ of the reference solution.

3. HIGH RESOLUTION INTERFACE CAPTURING (HRIC) SCHEME AND INTERFACE ANGLE CORRECTION

The High Resolution Interface Capturing (HRIC) scheme (Muzaferija and Perić 1998) describes the volume fractions α_C and α_f at cell center C and cell

face f, in terms of the volume fractions α_U and α_D of the next cell in upwind and downwind direction (U and D; cf. Fig. 1):

$$\tilde{\alpha}_C = \frac{\alpha_C - \alpha_U}{\alpha_D - \alpha_U}, \quad \tilde{\alpha}_f = \frac{\alpha_f - \alpha_U}{\alpha_D - \alpha_U} \quad . \tag{8}$$

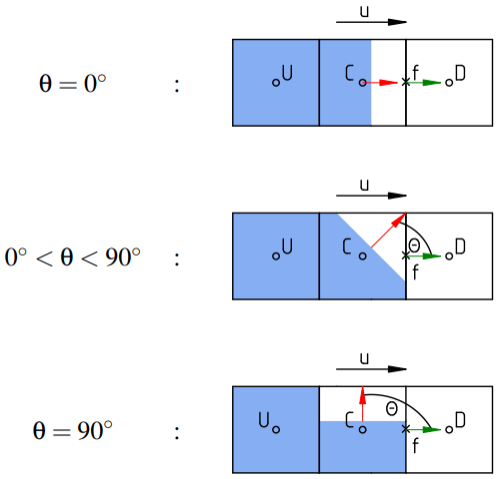

Fig. 1. One-dimensional volume fraction transport for different interface orientations θ with two phases indicated by blue and white shading; θ is the angle between interface normal (red) and cell face normal (green); cell centers of upwind, center and downwind cell relative to the velocity vector u, are denoted by U, C and D, respectively; for small Courant numbers, the flux through the cell face f can be approximated by the wetted part of the face.

In this way, the discretization of the normalized face value $\tilde{\alpha}_f$ can be defined only as a function of the cell value $\tilde{\alpha}_C$, the interface orientation θ (cf. Fig. 2 and, if Co > 0.3, of the Courant number Co. The latter is only included as a correction for large Co numbers, for which the discretization is blended towards first-order upwind to improve the stability (see Rapuc *et al.* 2018). In the present work held Co < 0.3, which is typically the case in high-accuracy flow simulations with free-surface waves, thus the influence of Co is not shown in Fig. 2 and also not further discussed.

The interface orientation is the angle θ between the normal vector of the free surface and the normal vector of the face under consideration as illustrated in Fig. 1. If θ approaches 90°, the face value α_f is obtained by first-order upwind differencing. This can be quickly understood by considering the fluxes of the blue shaded phase through cell face f in Fig. 1. If θ approaches 0°, then α_f is a mixture between α_C (upwind) and α_U (downwind), tending towards downwind when α_C tends towards 0.

The following blending function modifies the mixture between upwind and downwind differences as a function of θ:

$$\tilde{\alpha}_f^* = \tilde{\alpha}_f \cdot \cos(\theta)^{C_\theta} + \tilde{\alpha}_C \cdot [1 - \cos(\theta)^{C_\theta}] \quad . \tag{9}$$

A larger angle factor C_θ results in a curve closer to the diagonal in Fig. 2 and therefore a higher weighting of the first-order upwind differencing scheme. The influence of different angle factors for the simulation of free-surface waves is analyzed in the following sections.

4. SIMULATION SETUP

The numerical simulations are performed with the finite-volume-based flow solver Star-CCM+ 14.06.012 from Siemens. For the interface-capturing, the volume-of-fluid (VOF) method (Hirt and Nichols 1981) is used with the HRIC scheme (Muzaferija and Perić 1981) for interface-sharpening. The angle factor C_θ within the HRIC scheme is varied between 0 and 0.5 in steps of 0.05. Temporal discretization is of second-order accuracy and the time step is chosen low enough to result in Courant-numbers of Co < 0.3for all cases.

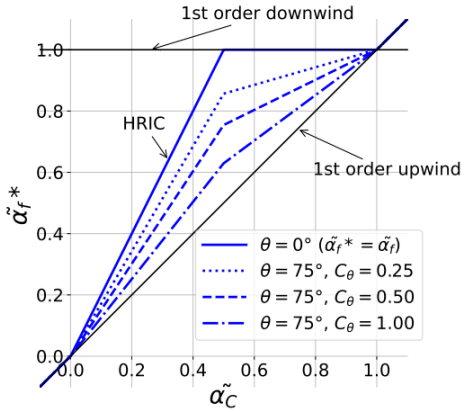

Fig. 2. Normalized-Variable Diagram for the HRIC scheme with the normalized corrected volume fraction on cell face $\tilde{\alpha}^*_f$, normalized volume fraction on cell center $\tilde{\alpha}_C$ and exemplary curves for their dependency for different interface orientations θ and angle factors C_θ; first order upwind and downwind schemes are included as black lines.

Long-crested regular free-surface waves with different wave height but the same wavelength $\lambda = 1.5m$ are simulated for wave steepnesses $H/\lambda = [0.0125, 0.05, 0.1]$ in terms of wave height H to cover a broad range from nearly linear waves until ca. 70% of the breaking steepness. Figure 3 shows the computational domain. The water depth of $h = 8/3\lambda$ results in *deep water* conditions ($h/\lambda > 0.5$). The coordinate system is set with its origin at the left side of the domain at stillwater level with the z-axis pointing positive upwards and x-axis pointing to the right. Waves traveling in positive x-direction are generated at the left side of the domain according to Stokes 5th-order wave theory. At the right boundary, a forcing zone with a width of 2λ is attached to minimize wave reflections. In the forcing zone, the solution for velocity $\boldsymbol{v}$ and volume fraction α is forced towards the reference solution for the calm

surface. The forcing strength $\gamma$and blending function $b(\boldsymbol{x})$ are optimized according to Perić (2019) with forcing strength of $\gamma = 7.5s^{-1}$ and exponential blending function

$$b(\boldsymbol{x}) = \left(\frac{e^{\left(\frac{x_d - \tilde{x}}{x_d}\right)^2} - 1}{e^1 - 1} \right) \quad , \tag{10}$$

where $\tilde{x}$ is the shortest distance of location $\boldsymbol{x}$ to the domain boundary to which a forcing zone of thickness x_d is attached.

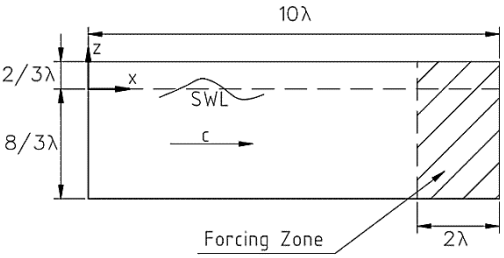

Fig. 3. Domain geometry with dimensions given as multiples of the wave length λ, position of the still water line (SWL) and wave phase propagation direction indicated by vector c; the forcing zone for wave damping is indicated by a hatched pattern.

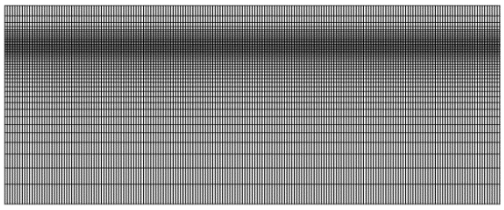

Fig. 4. Numerical grid for refinement level *very coarse* from Table 1.

Table 1 Mesh parameters; $f_{r,x}$ and $f_{r,z}$ denote the refinement factors in x- and z-direction, respectively - $f_{r,x}$ and $f_{r,z}$ indicates uniform mesh refinement

	Refinement factors		total number of cells
mesh	$f_{r,x}$	$f_{r,z}$	n_c
very coarse	1	1	9400
coarse	$1/\sqrt{2}$	$1/\sqrt{2}$	18678
medium	$1/2$	$1/2$	37600
fine	$1/(2\sqrt{2})$	$1/(2\sqrt{2})$	74712
very fine	$1/4$	$1/4$	150400
refined X 2.0	$1/2$	1	18800
refined X 4.0	$1/4$	1	37600
refined Z 2.0	1	$1/2$	18800
refined Z 4.0	1	$1/4$	37600

A block-structured grid with local mesh refinement as depicted in Fig. 4 is used. Near the water surface, the reference grid (*very coarse*) has 5 cells per wave height and 20 cells per wave length. The cell size gradually increases with increasing distance from the water surface. In y-direction, the grid is only one cell wide resulting effectively in a two-dimensional case.

Table 2 Mesh parameters near the free surface, with cell sizes $\Delta x$and Δz in x- and z-direction near the water surface, wave height H and wavelength λ

	cells per wave height	cells per wave length	aspect ratio
mesh	H/Δz	λ/Δx	Δx/Δz
very coarse	5	20	2.5
coarse	7	28.3	2.5
medium	10	40	2.5
fine	14	56.6	2.5
very fine	20	80	2.5
refined X 2.0	5	40	1.25
refined X 4.0	5	80	0.625
refined Z 2.0	10	20	5
refined Z 4.0	20	20	10

For the mesh sensitivity studies, differently refined meshes are generated based on the coarse mesh presented above (for mesh parameters see Table 1). Firstly, the mesh is uniformly refined in both x- and z-direction with refinement factors $1/\sqrt{2}$ (*coarse*), $1/2$ (*medium*), $1/(2\sqrt{2})$ (*fine*) and $1/4$ (*very fine*) meaning that the cell size in each direction is multiplied by the refinement factor. To analyze the influence of the cell aspect ratio, also nonuniformly refined meshes are created by refining the cells only in x-direction or only in z-direction by factors of $1/2$ and $1/4$ .The resulting mesh parameters near interface for all grids are presented in Table 2.

5. METHODS TO DETERMINE OPTIMUM PARAMETERS FOR THE INTERFACE SHARPENING SCHEME

This section proposes different methods to determine optimum parameters for the interface-sharpening scheme for the simulation of flows with free-surface waves. To assess the quality of the waves, different criteria are identified which will be presented in this section: The loss of wave height H/H_0, the interface distortion$\Delta H_{\max}$, the reflection coefficient C_R and the absolute vorticity$|\vec{\omega}|$. The wave height H required for the calculation of these parameters is calculated based on the vertical position of the free surface which is approximated by the isosurface for a volume fraction of $\alpha = 0.5$. Reflection coefficient C_R and vorticity $\vec{\omega}$ are analysed as parameters indicating optimum values for the case-dependent parameters C_θ of the HRIC interface-sharpening scheme. For these parameters, it will be shown that they include both the effects of wave height dissipation and interface distortion. The assessment

criteria derive from the main problems that occur for non-optimum blending of upwind and downwind differences which are the smearing of the interface and interface distortion (see section 1). Another possible assessment criterion not used in the present work is the loss of mechanical energy of the wave which includes the effects of changes in wave height.

Wave height dissipation results from smearing of the interface due to artificial diffusion. The wave height dissipation can be quantified as the ratio H/H_0 between measured wave height H at a designated distance from the wave inlet to wave height prescribed H_0 at the wave inlet. If H/H_0 is substantially smaller than 1, this can be an indicator for too diffusive interface-sharpening settings.

Interface distortion leads to the formation of surface irregularities with a magnitude smaller than the prescribed wave height H_0 and a horizontal extend smaller than the wavelength λ .These surface irregularities in FVM-based flow simulations were also reported and analysed by Larsen *et al.* (2019). Resulting from these surface irregularities, the results for local wave height H fluctuate over the wave propagation direction. The interface distortion can correspondingly be quantified by the ratio between the maximum wave height difference

$$\Delta H_{\max} = \max(H) - \min(H) \tag{11}$$

in a defined evaluation interval and the wave height H_0 prescribed at the inlet. This evaluation interval must extend over at least one wavelength λ in wave propagation direction. Results for the interface distortion obtained in this manner are determined here from wave height data cleaned of linear decline (as shown later in Fig. 5 - bottom) which might be due to wave height dissipation H/H_0 over the length of evaluation interval. In this way the interface distortion results exclude the influence of wave height dissipation over the length of the evaluation interval.

The results for both wave height dissipation H/H_0 and interface distortion $\Delta H_{\max}$ are obtained from the surface elevation in the designated evaluation interval between $x = 6\lambda$ and $7\frac{1}{3}\lambda$ from the inlet examined for a time interval of one wave period T starting after $t = 12.5T$ simulation time. The time interval is selected so that the wave energy, propagating with the group velocity $c_g = 0.5c$ (*deep water* conditions), in terms of phase velocity c, must have travelled from the wave inlet through the evaluation zone.

The *reflection coefficient* C_R is a measure of the wave reflection of at domain boundary and forcing zone. It is calculated as

$$C_R = \frac{\max(H)-\min(H)}{\max(H)+\min(H)} \quad , \tag{12}$$

with the maximum and minimum wave heights $\max(H)$ and $\min(H)$ that occur within the evaluation interval, for which the same interval as before is used. For the given setup, a reflection coefficient of $< 1\%$ can be expected due to close-to-optimum forcing in the forcing zone as described in section 4. and according to Perić and Abdel-Maksoud (2018) and Perić (2019). Interface distortion and wave height dissipation over the length of the evaluation zone however, result in larger reflection coefficients.

Vorticity can be produced by both interface disturbances and wave height dissipation as will be demonstrated in the following sections. For the two-dimensional case, it the vorticity is defined as

$$|\vec{\omega}| = |\omega_y| = \left|\frac{\partial u}{\partial z} - \frac{\partial w}{\partial x}\right|. \tag{13}$$

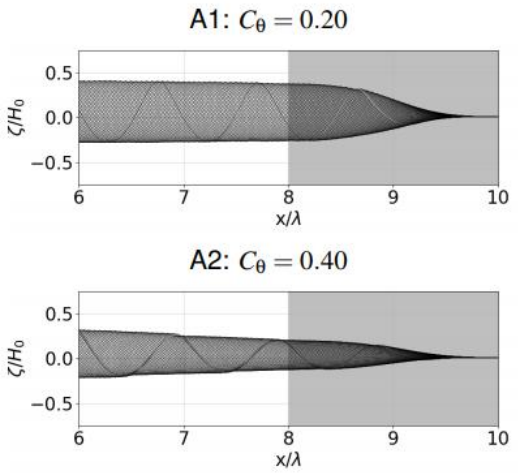

Fig. 5. Surface elevation ζ per prescribed wave height at inlet H_0 as a function of wave propagation direction x, for equally spaced time intervals over one wave period T near the forcing zone for wave damping (shaded in grey); plots correspond to points A1 and A2 in Fig. 7; if the angle factor C_θ is too large, the interface-sharpening leads to a substantial loss in wave height and energy.

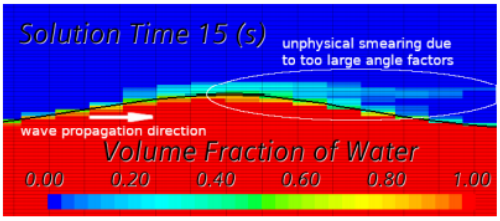

Fig. 6. Volume fraction α with angle factor $C_\theta = 0.40$ (point A3 in Fig. 8); an example of unphyshysical smearing of the interface due to too large C_θ values in the HRIC interface-sharpening scheme.

To exclude the effects of the forcing zone (starting at $x = 8\lambda$) and focus on the wave interface, the vorticity was averaged over the water phase from the wave inlet ($x = 0$) to x = $7\frac{1}{3}\lambda$, and from $z = -\frac{2}{3}\lambda$ upwards over the last period of simulation time.

1. RESULTS

Resulting from the surface elevations, the wave height dissipation (section 6.1), the interface distortion (section 6.2), the reflection coefficient (section 6.3) and the vorticity in the water phase near the free surface (section 6.4) are presented.

6.1 Wave Height Dissipation

Over the comparatively short wave propagation distances considered in the work, the wave should theoretically maintain its height and energy (Clauss *et_al.* 1992). However, discretization and iteration errors typically dissipate some wave energy; this effect vanishes on infinitely refined grids, but for practical discretizations a loss of wave height of a few percent is typical (see e.g. Rapuc *et al.* 2018). The results in this section demonstrate that the interface-sharpening scheme can also lead to substantial dissipation of wave height and energy, if its parameters are not optimized.

In Fig. 7 and 8, the results for wave height dissipation H/H_0 are presented for the three different waves with varying wave steepness and different mesh refinement levels from section 4. Figure 7 - 5 show that a larger angle factor C_θ increases the wave height

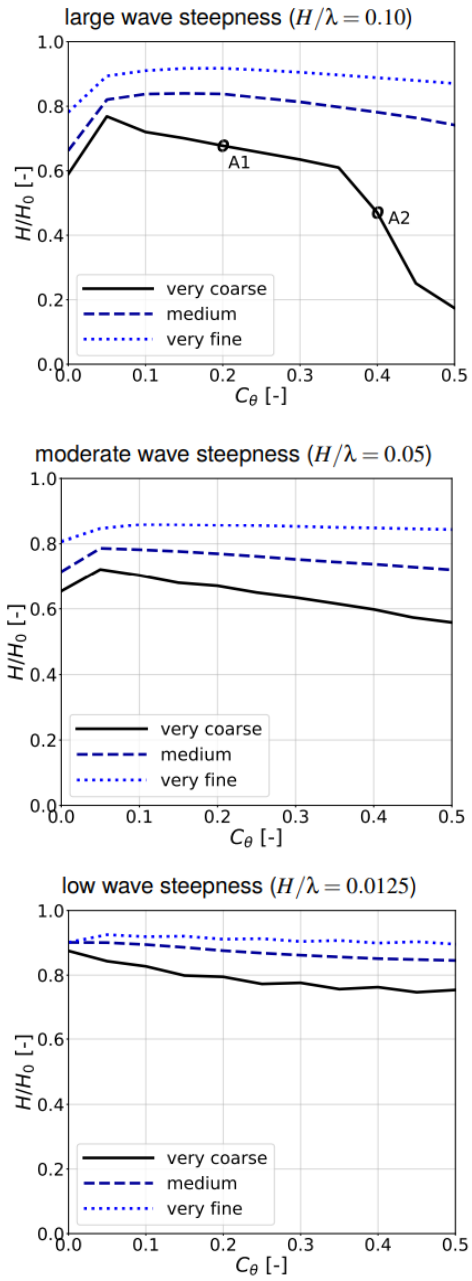

Fig. 7. Ratio between average wave height *H* in the evaluation zone and prescribed wave height H_0 at the wave inlet vs. angle factor C_θ for waves with different wave steepness *H/λ* and *uniform* mesh refinement (cf. Table 1).

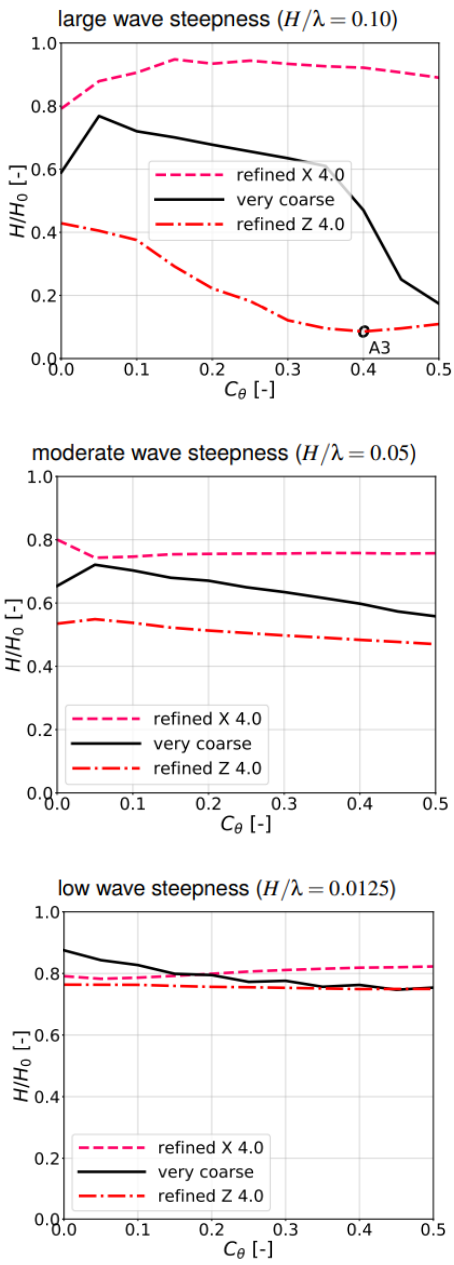

Fig. 8. As Fig. 7, except for *nonuniform* mesh refinement.

dissipation. Figure 6 shows that too large angle factors result in the volume fraction being advected

in horizontal direction faster than the propagation speed of the wave itself.

The upper two plots in Fig. 7 and 8 show that angle factors approaching to zero (no or small interface orientation correction) may also result in increased wave height dissipation which becomes more prominent with increasing wave steepness.

The uniform mesh refinement (Fig. 7) shows convergence towards the optimum solution (no wave height losses). A larger wave steepness results in a larger angle factor sensitivity: The coarser the mesh, the larger is the influence of the angle factor and the more important is a proper selection of this parameters.

The nonuniform refinement for cells with a smaller aspect ratio $\Delta x / \Delta z$ (*refined* X 4.0 in Fig. 8) produced lower wave height losses for the large and moderate steepness wave and lower or larger losses for the low steepness waves depending on the angle factor, indicating the optimum cell aspect ratio varies with wave steepness. However, cells with a larger aspect ratio on the other hand result in increased wave height losses for all wave steepnesses up to 90% (*refined* Z 4.0 in Fig. 8) in combination with a large angle factor C_θ, indicating that refining the grid does not necessarily reduce the errors due to incorrectly set-up interface-sharpening schemes.

It should be noted that the wave height dissipation simulated for all cases is rather large and better results can often be found in literature using a finer mesh. This paper however, focuses on practical relevant cases applicable also in 3D-simulations maintaining a reasonable computational effort.

6.2 Interface Distortion

This section demonstrates that, for lower-than-optimum C_θ values, the HRIC interface-sharpening scheme can generate undesired interface distortions, such as unphysical alignment of the free-surface with the mesh or the occurence of wriggles in the free-surface.

Figure 11 and 12 show the size of interface distortions as a function of the discretization and the interface-sharpening. In all simulations, the interface distortion $\Delta H_{\max}$ reduced with increasing angle factors C_θ, with the exception of relatively small fluctuations. Exemplary surface elevation plots presenting this phenomenon are given in Fig. 9. Extreme distortions can become visible in surface elevation and volume fraction field as shown in Fig. 10 at the right boundary. These extreme distortions appear due to alignment of the free-surface with the grid.

Uniform mesh refinement does not necessarily reduce the interface distortions (see Fig. 11).

Nonuniform refinement led to larger interface distortions the smaller the cell aspect ratio $\Delta x / \Delta z$ (see mesh *refined X4.0* in Fig. 12) for the large and low steepness wave as well as for the moderately steep wave with small values of C_θ. Otherwise, the interface distortion was in the range of $1-3\%$.

Increasing wave steepness H/λ amplified the interface distortion and increased the angle factor dependency which coincides with the observations regarding wave height dissipation in section 6.1.

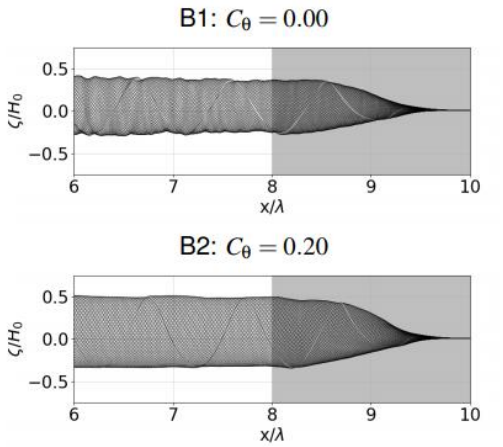

Fig. 9. Surface elevation ζ per prescribed wave height at inlet H_0 as a function of wave propagation direction x, for equally spaced time intervals over one wave period T near the forcing zone for wave damping (shaded in grey); plots correspond to points B1 and B2 in Fig. 11; if the angle factor C_θ is to small, the interface-sharpening leads to substantial interface distortions.

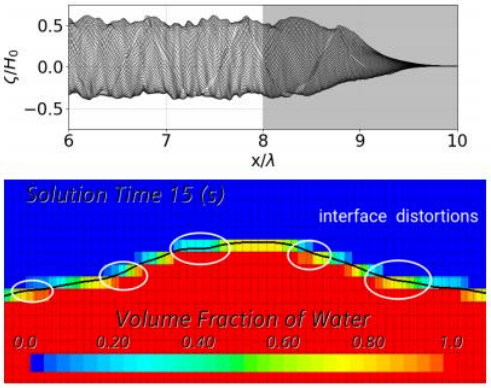

Fig. 10. Surface elevation ζ per prescribed wave height at inlet H_0 as a function of wave propagation direction x for equally spaced time intervals over one wave period T for point B3 in Fig. 12 (top) and volume fraction a for an extract of the domain (bottom); an example of significant unphysical compression of the wave surface due to too small values of C_θ in the HRIC interface-sharpening scheme.

In Fig. 11 and 12, the wave height in the evaluation zone varied at least by $1-2\%$, i.e. the wave was not perfectly regular. However, these variations were lower than one cell size and, apart from the interface-sharpening, there are also other mechanisms (inlet and outlet boundary conditions, initialized solution, etc.) that could have caused these comparatively small fluctuations. Thus $1-2\%$ wave height variations in the figures could be considered as

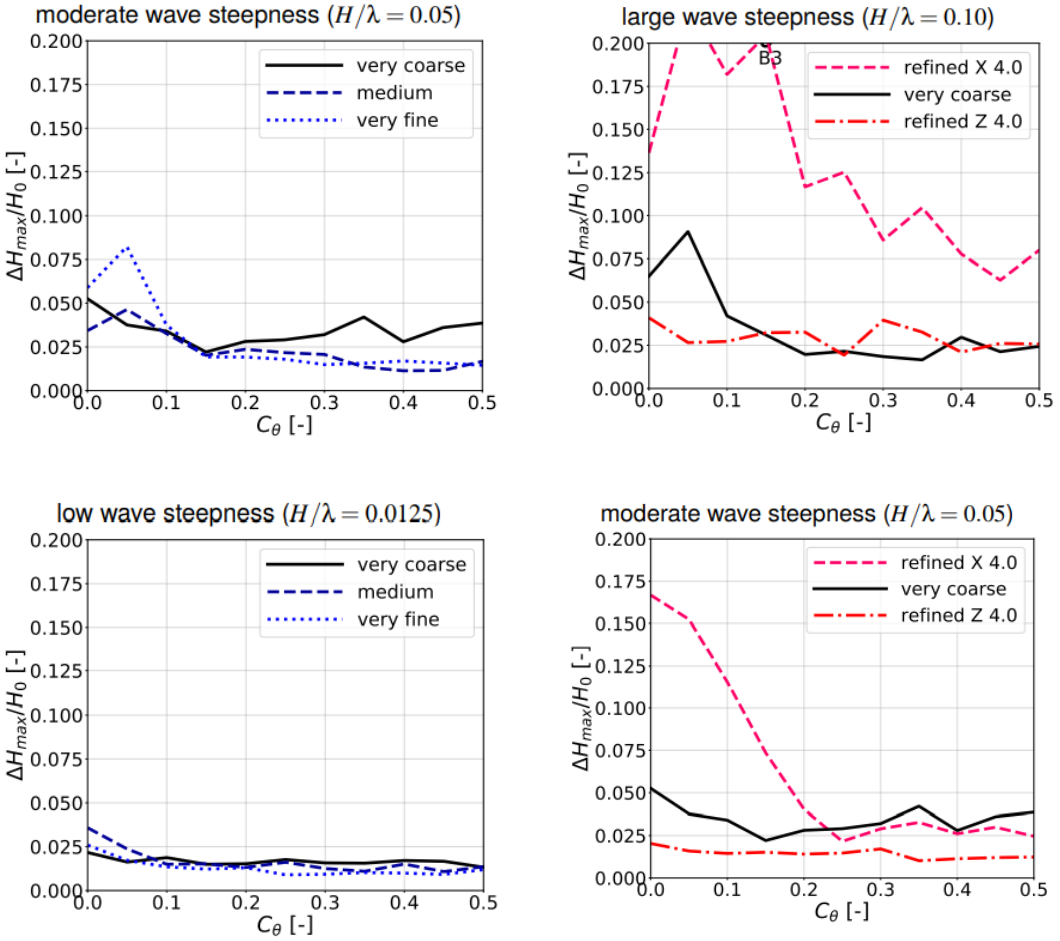

Fig. 11. Ratio between maximum wave height difference ΔH_{max} = max(H)−min(H) and prescribed wave height H_0 at the wave inlet vs. angle factor C_θ for waves with different wave steepness H/λ and *uniform* mesh refinement (cf. Table 1)

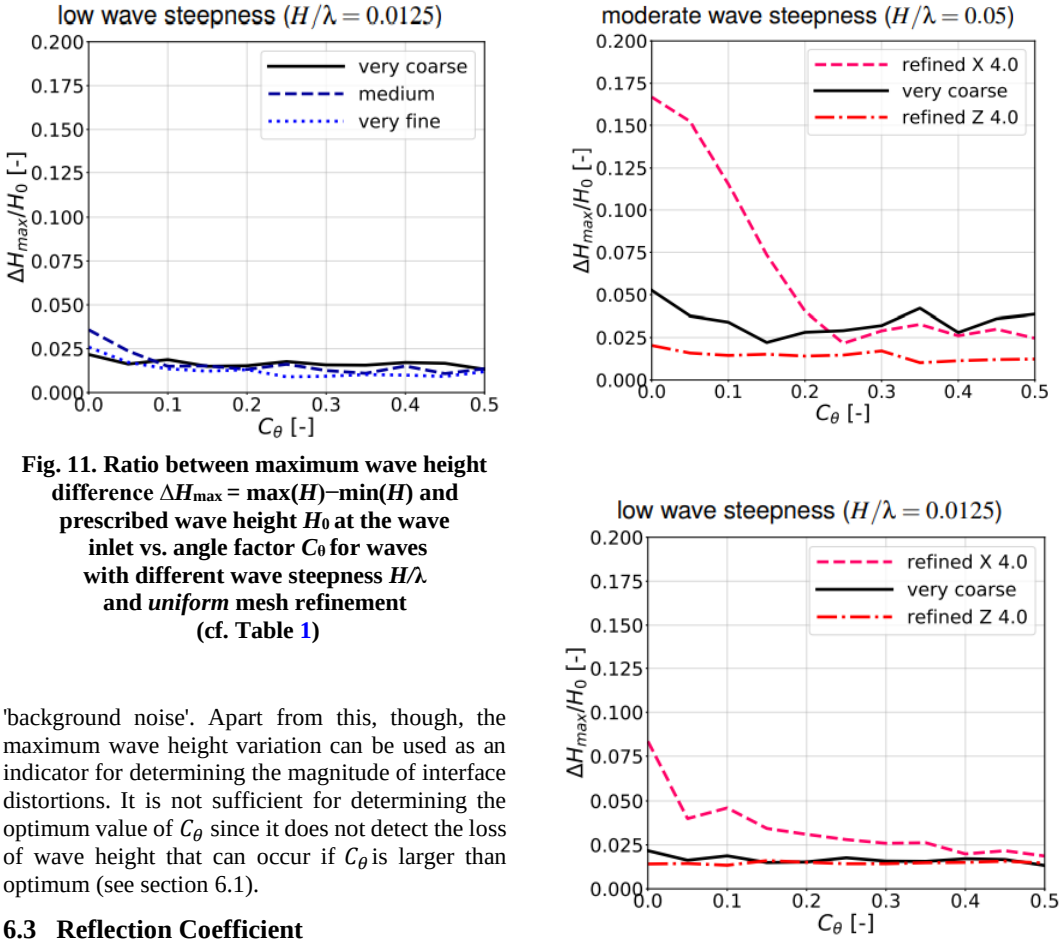

Fig. 12. As Fig. 11, except for *nonuniform* mesh refinement.

'background noise'. Apart from this, though, the maximum wave height variation can be used as an indicator for determining the magnitude of interface distortions. It is not sufficient for determining the optimum value of C_θ since it does not detect the loss of wave height that can occur if C_θ is larger than optimum (see section 6.1).

6.3 Reflection Coefficient

Figure 13 and 14 show that the value for the angle factor C_θ, which results in a minimum reflection coefficient C_R, depends on both wave steepness H/λ and on the mesh refinement level.

Uniform mesh refinement mostly reduced the reflection coefficient and shifted the minimum towards larger angle factors C_θ (see Fig. 13). For the steepest wave, the reflection coefficient shows a sudden increase for coarse meshes and angle factors $C_\theta > 0.35$. This was due to a rapid decline of the wave height over the length of the evaluation zone as can be seen also in Fig. 5 - bottom.

The results show that, for a simulation setup where C_R should theoretically be roughly zero, it can serve as a means to determine the optimum value for C_θ (limited by ca. $1-2\%$ background noise as in the previous section). Since C_R increases when C_θ becomes too large, the minimum of C_R provides an estimate of the optimum C_θ. Angle factors resulting in minimum reflection coefficients are summarized in Table 3 for the large steepness wave.

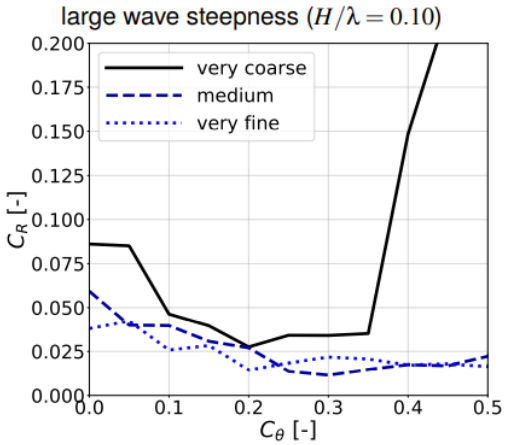

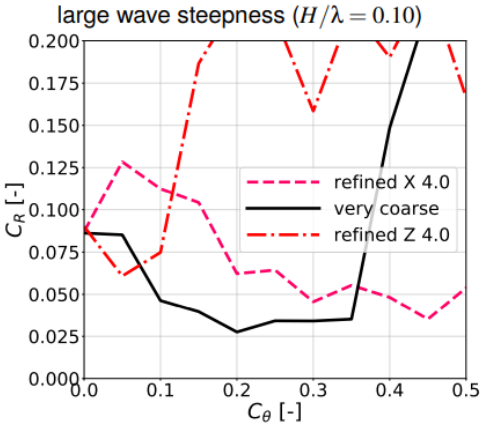

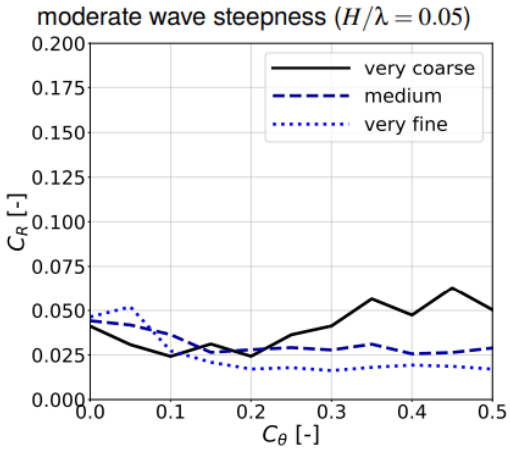

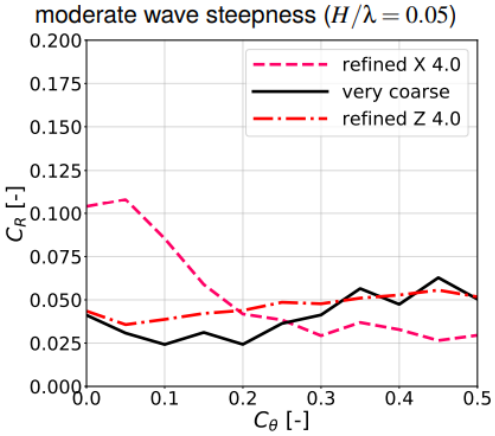

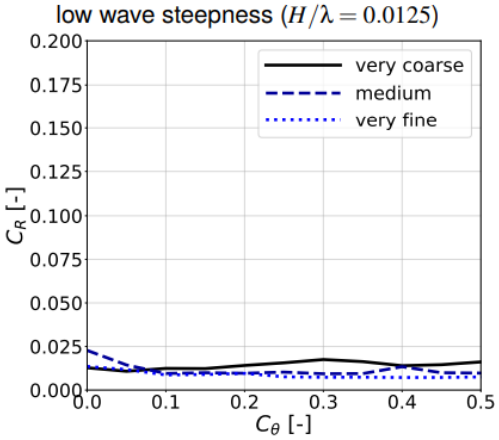

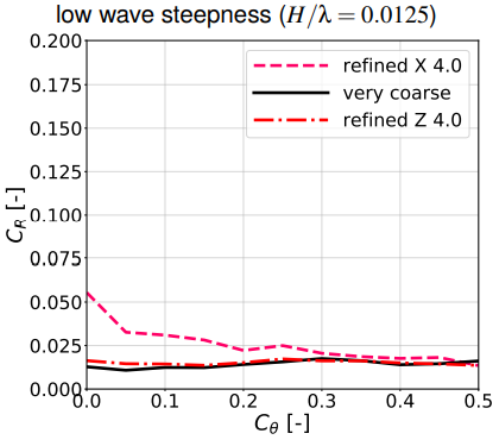

Fig. 13. Wave reflection coefficient C_R vs. angle factor C_θ for waves with different wave steepness H/λ and *uniform* mesh refinement (cf. Table 1)

Fig. 14. As Fig. 13, except for *nonuniform* mesh refinement.

The minimum reflection coefficient provides a trade-off between minimizing wave height dissipation and interface distortions. This is only valid for cases where theoretically no reflection must occur.

6.4 Vorticity

According to theory, a vorticity-free solution is expected for the velocity field of the undisturbed wave. Both interface disturbances and wave height dissipation can produce vorticity within the wave as demonstrated in Fig. 15 - 17. Therefore, section 6.4 investigates whether the vorticity within the wave can be used to determine the optimum value of C_θ.

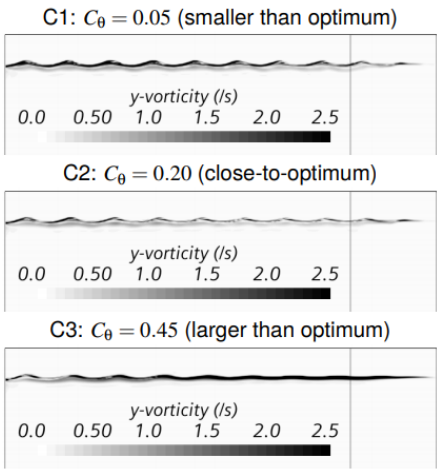

Fig. 15. Absolute vorticity $|\omega_y|$ around the y-axis in the fluid phase with the vertical line on the right side of the domain indicating the beginning of the forcing zone; the presented plots correspond to the cases marked by C1 to C3 in Fig. 16.

Table 3 Angle factors $C_{\theta,\,CRmin}$ resulting in minimum reflection coefficient C_R including variations of ±0.5% for different mesh refinement levels and different steepnesses H/λ in terms of wave height H and wavelength λ

	H/λ		
mesh	0.1	0.05	0.0125
uniform refinement			
very coarse	0.2	0.1...0.2	0...0.45
coarse	0.35...0.45	0.05	0...0.5
medium	0.25...0.35	0.15...0.5	0.1...0.5
fine	0.1...0.5	0.2...0.5	0.05...0.5
very fine	0.2...0.5	0.15...0.5	0.05...0.5
nonuniform refinement			
refined X 2.0	0.45	0.3...0.5	0.4...0.5
refined X 4.0	0.05	0.05...0.1	0.3...0.5
refined Z 2.0	0.1	0.05...0.25	0...0.5
refined Z 4.0	0.05	0.05...0.1	0...0.5

The vorticity results, nondimensionalized by division by $\frac{H_0}{c}$ in terms of wave height at the inlet H_0 and phase velocity c , are presented in Fig. 16 and 17. Table 4 lists the angle factors which resulted in minimum or close-to-minimum vorticity with a given tolerance. Figure 15 presents the vorticity contours for different angle factors C_θ with C_θ smaller than, close-to- and larger than optimum (from top to bottom). For the largest wave steepness (upper plot) in Fig. 16 and 17, the minima of the vorticity magnitude agree well with close-to-minimum values of the reflection coefficient C_R in Fig. 13 and 14; thus both proposed indicators successfully and with good consistency predicted the optimum value for C_θ , so that both interface disturbances and the loss of wave height and energy due to the interface-sharpening scheme were minimized. However, for the moderate and low wave steepness simulations, the vorticity magnitude decreased monotonically with increasing C_θ , and continued to decrease even when there was already a substantial loss of wave height. This can be partly explained because the vorticity in the wave is to some degree coupled to the wave energy, so when the wave energy is dissipated also the vorticity is reduced; therefore, the minimum vorticity magnitude may occur at larger values than the actual optimum of C_θ. Another reason may be that for lower wave steepnesses, the vorticity in the wave was also lower and the wave parameters were less affected by the choice of C_θ.

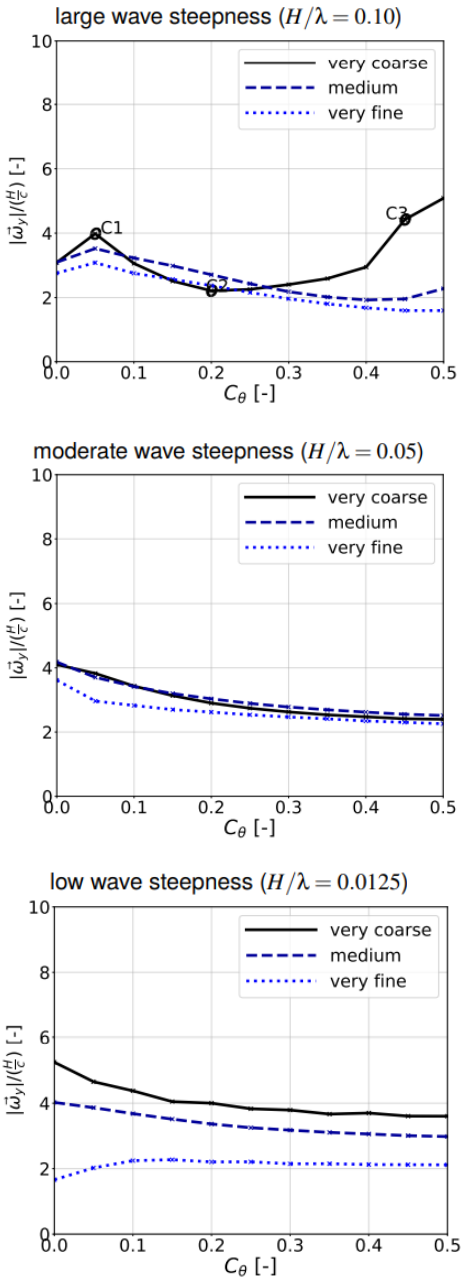

Fig. 16. Average *y*-vorticity in fluid phase in the test volume nondimensionalized with inlet wave height H_0 and phase velocity *c* vs. angle factor C_θ; results are presented for waves with different wave steepness H/λ and *uniform* mesh refinement (cf. Table 1).

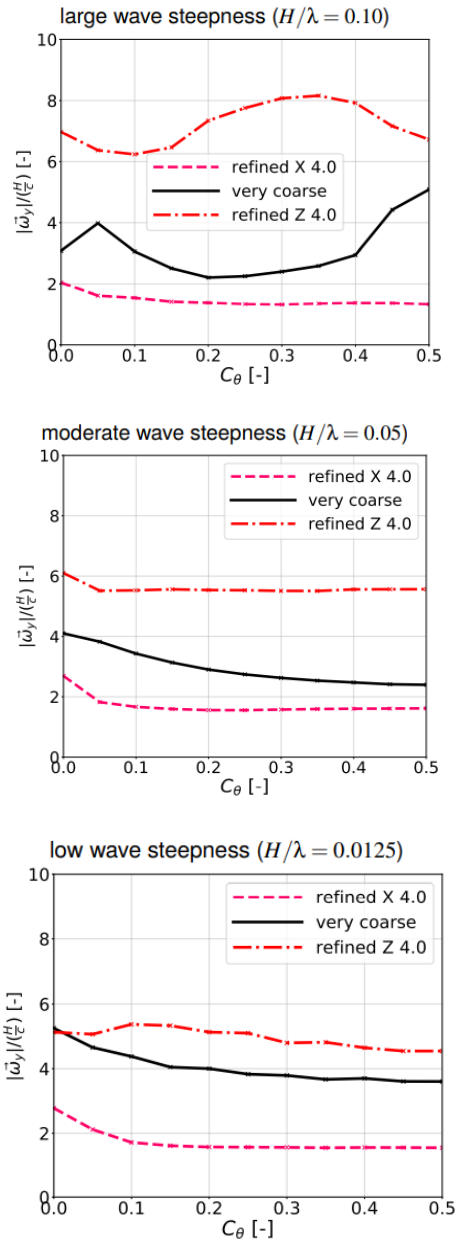

Fig. 17. As Fig. 16, except for *nonuniform* mesh refinement.

Table 4 Angle factors $C_{\theta,|\omega y|min}$ resulting in minimum vorticity magnitude $|\omega_y|$ including variations of ±0.02s^{-1} for different mesh refinement levels and different steepnesses H/λ in terms of wave height H and wavelength λ

	H/λ		
mesh	0.1	0.05	0.0125
uniform refinement			
very coarse	0.2...0.3	0.25...0.5	0.15...0.5
coarse	0.3...0.4	0.3...0.5	0.2...0.5
medium	0.35...0.45	0.3...0.5	0.15...0.5
fine	0.35...0.5	0.4...0.5	0...0.5
very fine	0.35...0.5	0.4...0.5	0...0.5
nonuniform refinement			
refined X 4.0	0.15...0.5	0.05...0.5	0...0.5
refined X 2.0	0.05...0.5	0.05...0.5	0...0.5
refined Z 2.0	0.15...0.25	0.1...0.5	0.05...0.5
refined Z 4.0	0.1	0.05...0.5	0...0.5

Figure 17 shows that the influence of the cell aspect ratio was large. An increased aspect ratio $\Delta x / \Delta z$ substantially increased the vorticity whilst a small aspect ratio tended to reduce vorticity.

1. DISCUSSION

An appropriate selection of the angle factor is always a trade-off between wave height diffusion and interface distortion. The present results indicate that C_R can be used to estimate the optimum angle factor since the reflection coefficient includes by definition both the effects from wave height dissipation and interface distortion. A low value of C_R for a setup where no substantial wave reflection is expected implies that both interface-distortions and unphysical loss of wave height were minimized and that the angle factor was selected close to its optimum value for the investigated case. For steep waves, the vorticity magnitude $|\vec{\omega}|$ also provided an acceptable estimate of the optimum angle factor $C_{\theta,\mathrm{opt}}$. However, for the investigated moderate and low steepness waves, the vorticity magnitude over-estimated $C_{\theta,\mathrm{opt}}$, since loss in wave energy due to overly-diffuse interface-sharpening produced a loss in vorticity. Because free-surface wave propagation is typically a nearly inviscid phenomenon, evaluating the vorticity can nevertheless be useful to determine the suitability of the simulation setup, with preference towards lower vorticity values. Loss of wave height and interface-disturbances can be quantified by H/H_0 and ΔH_{max}, respectively, and can be used as an indicator of the suitability of the simulation setup, but they do not predict the optimum parameters of the interface-sharpening scheme. Although the present investigation was performed only for the HRIC scheme, the main conclusions from the present work, especially regarding the proposed techniques to optimize the case-dependent parameters, will apply to all NVD-based interface-sharpening schemes.

A certain loss of wave height is often acceptable. While it could be minimized by refining the discretization, if the loss is sufficiently small (a few percent), it is more efficient to increase the wave height at the inlet accordingly so that at the location of interest within the domain the desired wave height is obtained. If possible, it is preferable to optimize the numerical discretization with the angle factor over increasing the wave height at the inlet especially for large computational domain as this might lead to changes in wave dispersion or wave breaking.

The results show that wave height dissipation and interface distortion depend also on wave steepness. Their magnitude and their sensitivity to the angle factor both increase for steeper waves. It can be concluded that optimizing the case-dependent parameters becomes more necessary with increasing wave steepness.

Uniform mesh refinement resulted in smaller loss of wave height but not necessarily in less interface-distortion. The drawback of mesh refinement is the increased computational effort especially for 3D-simulations.

Nonuniform mesh refinement in some cases even increased the interface disturbances and the loss of wave height, demonstrating that mesh refinement is not generally suitable.

2. CONCLUSION

The HRIC scheme includes the user-defined parameter angle factor C_θ influencing the discretization of the volume fraction. If C_θ is not optimally selected, in the simulation of free surface waves wave height dissipation and interface distortions cas occur, which can produce substantial errors in the results (local changes in wave height of 20% or more resulting in 44% or more changes in wave induced forces). Theoretical considerations suggest that these problems will occur for other NVD-based interface-sharpening schemes as well. A systematic procedure was presented to determine the optimum value for C_θ via computationally inexpensive 2D-flow simulation based on determining the value of reflection coefficient C_R. Alternatively, the vorticity magnitude $|\vec{\omega}|$ can also be used to provide an estimate of close-to-optimum settings for C_θ; however for moderate and low steepnesses the vorticity magnitude over-estimated the optimum C_θ value, so that the reflection coefficient is more suitable.

Based on the present results it is recommended, if the interface disturbances or an unacceptable loss of wave energy occur in a flow simulation, to perform a parameter study with computationally efficient 2D-flow simulations as outlined in this work and to determine the most suitable choice for the mesh aspect ratio and the angle factor (or presumably the corresponding case-dependent parameters in other NVD-based interface-sharpening schemes) based on the results for the reflection coefficient as outlined in this work.

ACKNOWLEDGMENTS

The authors gratefully acknowledge the financial support by the Deutsche Forschungsgemeinschaft (DFG) (project AB 112/11-2) for this study.

REFERENCES

Clauss, G., E. Lehmann and C. Öestergaard (1992). *Offshore structures*, Springer.

Darwish, M. and F. Moukalled (2006). Convective Schemes for Capturing Interfaces of Free-Surface Flows on Unstructured Grids. *Numerical Heat Transfer, Part B: Fundamentals* 49(1), 19-42.

Hirt, C. W. and B. D. Nichols (1981). Volume of fluid (VOF) method for the dynamics of free boundaries. *Journal of Computational Physics* 39(1), 201-225.

Lafaurie, B., C. Nardone, R. Scardovelli, S. Zaleski and G. Zanetti (1994). Modelling Merging and Fragmentation in Multiphase Flows with SURFER. *Journal of Computational Physics* 113, 134-147.

Larsen, B. E., D. R. Fuhrman and J. Roenby (2019). Performance of interFoam on the simulation of progressive waves, *Coastal Engineering Journal* 61, 380-400.

Leonard, B. P. (1991). The ULTIMATE conservative difference scheme applied to unsteady one-dimensional advection, *Computer Methods in Applied Mechanics and Engineering* 88, 17-74.

Muzaferija, S., M. Perić, P. Sames and T. Schelin (1998). A two-fluid Navier- Stokes solver to simulate water entry, In *Proceeding of Twenty-Second Symposium on Naval Hydrodynamics*

Ni, X., W. Feng, S. Huang, X. Zhao and X. Li (2020). Hybrid SW-NS SPH models using open boundary conditions for simulation of free-surface flows, *Ocean Engineering* 196,106845

Perić (2019). *Minimizing undesired wave reflection at the domain boundaries in flow simulations with forcing zones*. Doctoral dissertation, Technical University of Hamburg, Germany.

Perić, R. and M. Abdel-Maksoud (2018). Analytical prediction of reflection coefficients for wave absorbing layers in flow simulations of regular free-surface waves. *Ocean Engineering* 147, 132-147.

Rapuc, S., P. Crepier, F. Jaouen, T. Bunnik and P. Regnier (2018). Towards guidelines for consistent wave propagation in CFD simulations. *NAV International Conference on Ship and Shipping Research*, 515-524.

Ubbink, O. and R. I. Issa (1999). A Method for Capturing Sharp Fluid Interfaces on Arbitrary Meshes. *Journal of Computational Physics* 153, 26-50.

Wacławczyk, T. and T. Koronowicz (2008). Comparison of CICSAM and HRIC highresolution schemes for interface capturing. *Journal of Theoretical and Applied Mechanics* 46, 325-345.

Zheng, Z., G. Duan, N. Mitsume, C. Shunhua and S. Yoshimura (2020). A novel ghost cell boundary model for the explicit moving particle simulation method in two dimensions. *Computational Mechanics* 102, 66-87

.